Eur. Phys. J. D **27**, 273–276 (2003)
DOI: 10.1140/epjd/e2003-00275-5

THE EUROPEAN PHYSICAL JOURNAL D

Non-linear Sagnac interferometry for pump-probe dispersion spectroscopy

G. Jundt[a], G.T. Purves, C.S. Adams, and I.G. Hughes

Department of Physics, Rochester Building, University of Durham, South Road, Durham, DH1 3LE, UK

Received 5 June 2003
Published online 16 September 2003 –

Abstract. We explore pump-probe non-linear Sagnac interferometry as a tool to measure the dispersive properties of a medium. We introduce the background theory, and show experimental spectra obtained on the D_2 transition with ^{85}Rb and ^{87}Rb. The measured dispersion spectra are in excellent agreement with the Kramers-Kronig relations. In addition, as both beams traverse identical optical paths, Sagnac interferometry is very robust against mechanical vibration

PACS. 39.30.+w Spectroscopic techniques – 33.55.Ad Optical activity, optical rotation; circular dichroism

1 Introduction

Doppler-free spectroscopy [1] of atomic media has become a standard technique in many important research areas such as laser cooling and metrology. However, whereas measurements of Doppler-free absorption are commonplace, measurements of the concomitant dispersion spectra are relatively rare. Recently, there has been renewed interest in the dispersive properties of atoms following experiments on sub- [2] or super-luminal [3] propagation of weak probe pulses. These effects are related to electromagnetically induced transparency (EIT) [4,5]. The key feature of EIT is a narrow transmission window within the usual absorption lineshape. Associated with this window is a rapid variation in the refractive index. Direct measurements of the dispersive spectrum typically requires some form of interferometry, such as a Mach-Zehnder interferometer [6]. However, a problem with this arrangement is that small vibrations of the optical components lead to intensity changes in the output, and active stabilisation of the interferometer is required. Measurement of the dispersion of an atomic medium could also provide an ideal reference signal for "locking" a laser to a particular atomic resonance [7]. In common with other differencing methods, such as polarization spectroscopy [8,9], and magnetically induced dichroism [10–12], dispersion spectroscopy has the advantage that the laser frequency does not need to be "dithered" [13]. An additional advantage of dispersive signals is that they fall away less quickly with detuning from line centre (as the inverse of the detuning compared with the inverse of the detuning cubed for a derivative lineshape).

In this paper, we show that Sagnac interferometry is ideally suited to measure the dispersion of an atomic medium. In Sagnac interferometry both beams traverse the same path, so the output is not sensitive to vibration of the optical components. We demonstrate the use of the Sagnac interferometer to measure the dispersion of a thermal rubidium vapour in a non-linear pump-probe experiment. In a previous experiment using a Sagnac interferometer [7], the interferometer was deliberately misaligned and a split photodiode was used to detect the "tilt" error signal. In contrast, we adapt a method developed for polarization spectroscopy [9] where both output ports are detected. In this case, there is no misalignment and the dispersive component is obtained from the difference signal between the two Sagnac output ports. By comparing the absorption and refractive index using the Kramers-Kronig relations we show that this method produces a nearly pure dispersive signal.

The paper is organised as follows: Section 2 outlines the theory of the non-linear Sagnac interferometer; in Section 3 we discuss the experimental details. Section 4 presents the results, and discusses their significance; finally, Section 5 concludes our findings and presents possible extensions to this work.

2 Theory

The geometry of the Sagnac interferometer is shown in Figure 1. The incident beam is split into two by a 50:50 beam splitter. The two beams travel through the vapour cell in opposite directions and then recombine on the beam

[a] *Present address*: Institute of Quantum Electronics, Department of Physics, ETH Zürich, Hönggerberg 8093, Switzerland. e-mail: i.g.hughes@durham.ac.uk

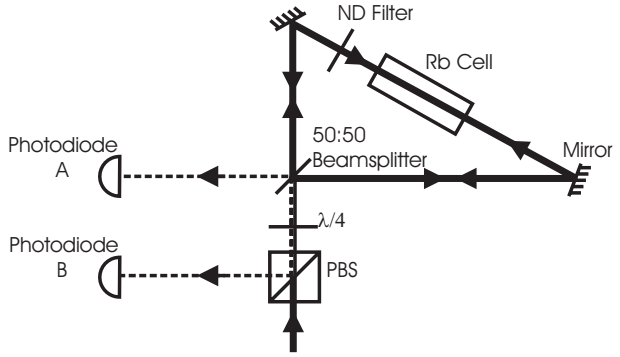

Fig. 1. Experimental set-up. The incident linearly polarized beam is transmitted by the polarizing beam splitter (PBS), and converted into circularly polarized light by the quarter-wave plate. The 50:50 beam splitter separates the input into a probe, which traverses the neutral density filter (ND) before the cell, and a pump, which traverses the cell first. The pump and probe interfere at the 50:50 beam splitter, and the intensities of the two output ports are recorded by photodiodes A and B. The output beam that retraces the path of the input is reflected by the PBS.

splitter. The output beams are detected by two photodiodes. Both beams pass along the same paths, so the interferometer is not sensitive to vibrations of the optical components. Also both beams experience the same phase shifts so no interference fringes are observed. However, if we introduce an asymmetry by placing a neutral density filter on one side of the vapour cell, we then have a weak "probe" beam traversing the cell in one direction and a strong "pump" beam passing through the cell in the other direction, similar to the arrangement in standard saturation spectroscopy. On account of the intensity dependence of the absorption of the medium we also expect an intensity dependent phase shift. This intensity dependence is crucial for obtaining fringes in the Sagnac interferometer. Essentially the non-linearity in the absorption process means that the sequence vapour cell — attenuator and attenuator — vapour cell do not commute.

As indicated in Figure 1 both outputs of the interferometer, labelled A and B, are monitored. The signals of interest are obtained by adding and subtracting the individual intensities. We now show that the difference between the individual ports is an excellent approximation to the refractive index of the medium. The intensities at photodiode A can be expressed as

$$\frac{I_{\rm A}}{I_0} = \frac{t^2}{4}\left|{\rm e}^{-\alpha_1 L/2}{\rm e}^{{\rm i}(kn_1L+\phi_{1\rm A})} + {\rm e}^{-\alpha_2 L/2}{\rm e}^{{\rm i}(kn_2L+\phi_{2\rm A})}\right|^2 = \frac{t^2}{4}\left[{\rm e}^{-\alpha_1 L} + {\rm e}^{-\alpha_2 L} + 2{\rm e}^{-\alpha L}\cos(k\Delta nL+\phi_{\rm A})\right], \quad (1)$$

and similarly for B. In this expression, I_0 is the incident laser intensity, $\alpha_{1,2}$ and $n_{1,2}$ are the absorption and refractive index experienced by the pump and probe beams, respectively, $\Delta n = n_1 - n_2$, $\alpha = (\alpha_1 + \alpha_2)/2$, and k is the magnitude of the probe wavevector. The attenuation factor t corresponds to the ratio of pump to probe fields in the cell, which has length L. The factor 1/4 arises as each beam interacts with the 50:50 beam splitter twice. The difference between the phase shifts induced by reflection and transmission at the beam splitter are labelled $\phi_{\rm A} = \phi_{1\rm A} - \phi_{2\rm A}$, and similarly for B. Time-reversal symmetry and energy conservation lead to the following relations for the phase shifts [15]

$$\phi_{1\rm A} - \phi_{2\rm A} = \frac{\pi}{2} \quad \text{and} \quad \phi_{1\rm B} - \phi_{2\rm B} = -\frac{\pi}{2}. \quad (2)$$

Substitution into equation (1) leads to the following expressions for the sum and difference intensities of the two output ports, A and B:

$$I_{\rm A} + I_{\rm B} = I_0\frac{t^2}{2}\left({\rm e}^{-\alpha_1 L} + {\rm e}^{-\alpha_2 L}\right), \quad (3)$$

$$I_{\rm A} - I_{\rm B} = I_0 t^2\left[{\rm e}^{-(\alpha_1+\alpha_2)L/2}\sin(k\Delta nL)\right]. \quad (4)$$

The sum has no explicit dependence on the refractive index, whereas for the typical case of the argument of the sine being small (valid in our experiment), the difference signal is linearly proportional to the refractive index difference. The prefactor which depends on both the unmodified and modified absorption has a different spectral profile to the refractive index difference. However, for modest modifications of the absorption (which can always be achieved by using low intensity beams) the prefactor hardly alters the spectral profile of the dispersion arising from the refractive index difference, Δn. If the refractive index of a vapour is close to unity, the Kramers-Kronig formulae [14] can be used to relate the absorption coefficient (proportional to the imaginary part of the dielectric constant) to the refractive index (proportional to the real part of the dielectric constant).

For an alkali metal atom with nuclear spin, I, there are two hyperfine ground states: $F = I+1/2$ and $F = I-1/2$. For Rb, the atom used in the work presented here, there are two stable isotopes (^{85}Rb, $I = 5/2$, ^{87}Rb, $I = 3/2$) with the hyperfine splitting of the groundstates (3.0 GHz for ^{85}Rb, 6.8 GHz for ^{87}Rb) exceeding the room temperature Doppler width (500 MHz), whereas the excited state hyperfine splitting is less than the Doppler width. So the absorption spectrum consists of 4 isolated Doppler broadened absorption lines. The counter-propagating pump beam introduces sub-Doppler absorption features. There are three excited state resonances coupled to the ground state *via* electric dipole transitions, namely $S_{1/2}(F) \rightarrow P_{3/2}(F' = F+1, F, F-1)$. In addition, one observes three cross-over resonances, appearing halfway in frequency between each pair of conventional resonances. Consequently, we expect the refractive index spectrum to exhibit 6 sub-Doppler peaks on top of a broad background, arising from hyperfine pumping [16], for each of the four lines.

3 Experimental details

The experimental arrangement comprised two counter-propagating laser beams in a 50 mm long Rb cell, at

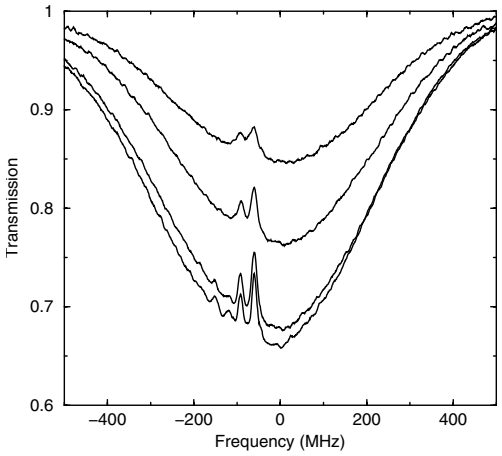

Fig. 2. Transmission spectra for the transition $5S_{1/2}(F = 3) \rightarrow 5P_{3/2}(F')$ in ^{85}Rb. The probe had a power of 50 μW and the pump had a power of 1.5 mW, 420 μW, 40 μW and 15 μW in order of decreasing transmission. The dependence of the absorption on laser power illustrates the non-linearity exploited in the interferometer. Six sub-Doppler features on a broader background are seen. The origin of the six features is explained in the text.

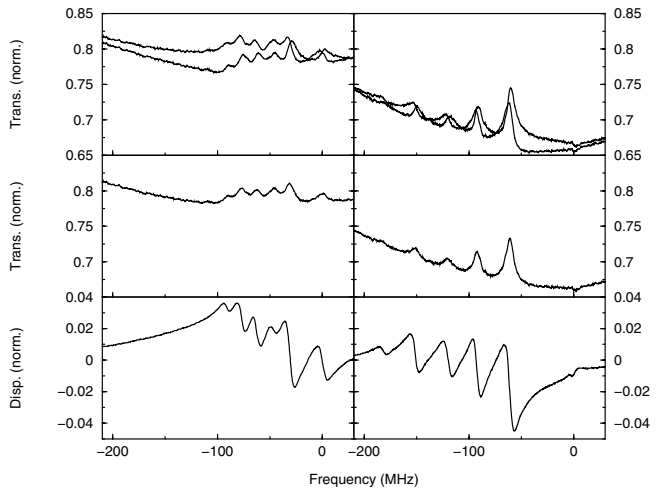

Fig. 3. The left and right columns show data from the $5S_{1/2}(F = 2) \rightarrow 5P_{3/2}(F')$ and $5S_{1/2}(F = 3) \rightarrow 5P_{3/2}(F')$ transitions in ^{85}Rb, respectively. The top row shows the outputs recorded by photodiodes A and B; the middle row shows the sum of the outputs, which is a transmission spectrum; the bottom row shows the difference between the readings of photodiodes A and B, which is the refractive index difference. The pump and probe powers were approximately 6 μW and 60 μW respectively, and the beam diameter was 3 mm in each case.

room temperature, $T = 293$ K. The cell was tilted slightly from the normal with respect to the beams to avoid feedback into the laser. The laser beams were derived from a home-built extended cavity diode laser and tuned to scan across the D_2 transition. A polarizing beam splitter and a quarter-wave plate were used to achieve counter-propagating beams, and to separate the input beam from one of the output beams by ensuring that the interference signal is reflected by the polarizing beam splitter instead of being transmitted along the direction of the input beam. Both pump and probe beams had circular polarization in the cell. Both beams had a diameter ($1/e^2$) of approximately 3 mm.

4 Results and discussion

To verify that indeed it is possible for the pump and probe beams, with our parameters, to experience different absorption we performed a preliminary experiment. Figure 2 shows the absorption spectrum when the laser is scanned by ± 500 MHz across the $5S_{1/2}(F = 3) \rightarrow 5P_{3/2}(F' = 4, 3, 2)$ transitions for ^{85}Rb. The different traces correspond to different beam powers. It is clearly evident that the absorption of the medium is dependent on the power of the pump beam. Six sub-Doppler features are clearly visible. In contrast to polarization spectroscopy [9], where the closed transition $5S_{1/2}(F = 3) \rightarrow 5P_{3/2}(F' = 4)$ dominates, the strongest features are two of the three cross-over resonances.

Figure 3 shows the raw results obtained for $5S_{1/2}(F = 2) \rightarrow 5P_{3/2}(F')$ transitions for ^{85}Rb and $5S_{1/2}(F = 3) \rightarrow 5P_{3/2}(F')$ transitions for ^{85}Rb. The upper row shows the traces obtained from both output ports of the interferometer. The middle row shows the sum of the two output ports, which are very similar to a conventional saturated absorption/hyperfine pumping spectrum, as predicted by equation (3). The bottom row shows the difference between the two output ports, clearly showing six dispersion lineshapes embedded in a slowly varying background. The dispersion signal is normalised by dividing by the intensity in one port. For a photodiode signal of a few volts the difference signal is a few hundred milli-volts.

For ease of comparison with the Kramers-Kronig equations we subtract the slowly varying background from the traces. This is done by obtaining a coarse average of the spectra, over a frequency scale which averages out the sub-Doppler features, and subtracting this to leave only the six narrow features. Figure 4 shows the dispersion spectra of both isotopes from both hyperfine groundstates. The thick line corresponds to the measured signal, and the thin line is calculated from the absorption data using the Kramers-Kronig formula. We do not predict the absorption and dispersion spectra theoretically for this comparison, rather the input for the Kramers-Kronig integral is the measured absorption, and we evaluate the integral to calculate the expected dispersion. Only one free parameter, the vertical scaling, is used. This parameter was chosen such that the largest peak in each spectrum matches with the experimental data. For all four data sets the experimental spectra are in excellent agreement with the Kramers-Kronig prediction. This shows that, at the power levels studied in Figure 4, the Sagnac method provides an excellent probe of the dispersion. However, as the beam intensities are important parameters in the experiment, we have also studied what happens at higher pump and probe powers.

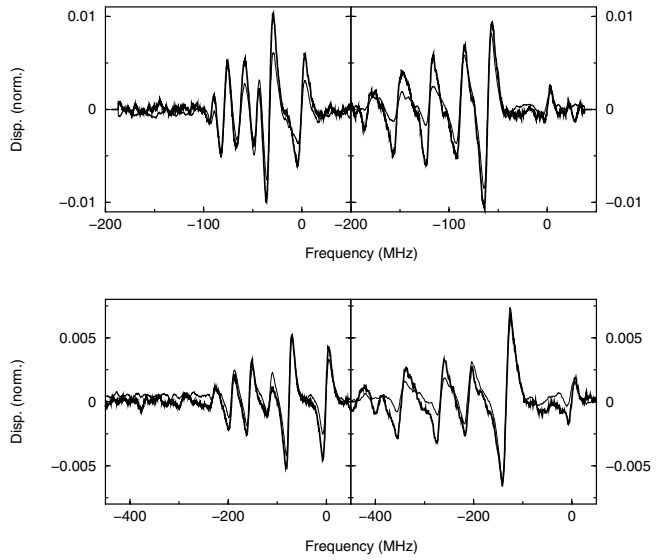

Fig. 4. The upper left and right curves show the $5S_{1/2}(F = 2) \rightarrow 5P_{3/2}(F')$ and $5S_{1/2}(F = 3) \rightarrow 5P_{3/2}(F')$ transitions in ^{85}Rb, respectively. The lower left and right curves show the $5S_{1/2}(F = 1) \rightarrow 5P_{3/2}(F')$ and $5S_{1/2}(F = 2) \rightarrow 5P_{3/2}(F')$ transitions in ^{87}Rb, respectively. The thin line shows the corresponding Kramers-Kronig prediction derived from the absorption spectrum. The probe and pump powers were approximately 2 μW and 12 μW respectively, and the beam diameter was 3 mm.

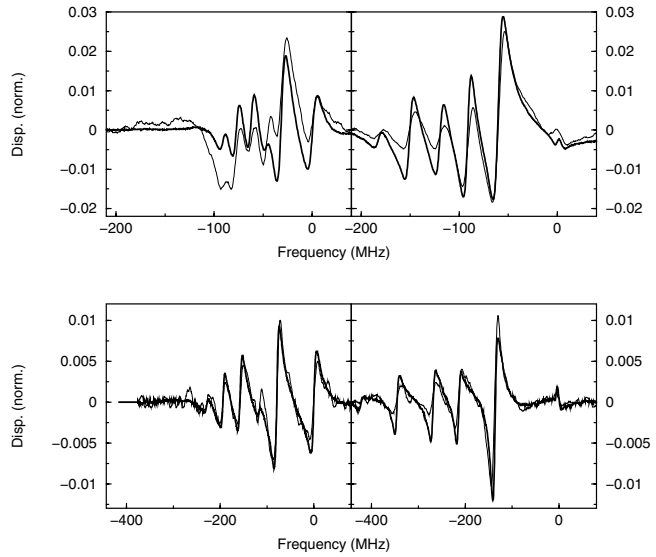

Fig. 5. The same spectra as in Figure 4 but with pump and pump powers of approximately 6 μW and 60 μW respectively, and a beam diameter of 3 mm.

Figure 5 shows scans obtained when the pump and probe power are increased by a factor of 5 and 3, respectively. Although the features are stronger, there is a power-broadening of the lines which degrades the spectral resolution. This is seen in particular in the isotope ^{85}Rb (top row) where the agreement between the measured dispersion and the Kramers-Kronig prediction is less good. However, for ^{87}Rb where the excited state hyperfine splitting is larger, the broadening of the lines does not compromise the separation of the spectral features and the agreement remains excellent, as seen in the bottom row. The choice of laser power is therefore dependent on the particular application in mind.

5 Conclusion

In this paper, we have described the theory and performance of a non-linear Sagnac interferometer. We show that it provides an almost pure dispersive signal and unlike most other interferometers, is not sensitive to small variations in the optical path length. The relationship between the absorption and dispersion governed by the Kramers-Kronig relations was found to be in excellent agreement with the experimental data. Increasing the laser intensity served to increase the peak heights, but at the expense of broader lines and poorer spectral resolution. The dispersion spectra have a linear slope through the line centres (for small departure from the resonance frequency), and could be used for laser frequency locking. We plan to extend the work to measuring electromagnetically induced dispersion in the near future.

This work was supported by EPSRC and Durham University.

References

1. W. Demtröder, *Laser spectroscopy* (Springer-Verlag, 1996)
2. L.V. Hau, S.E. Harris, Z. Dutton, C.H. Behroozi, Nature **397**, 594 (1999)
3. L.J. Wang, A. Kuzmich, A. Dogariu, Nature **406**, 277 (2000)
4. E. Arimondo, Progr. Opt. **XXXV**, 257 (1996)
5. J.P. Marangos, J. Mod. Opt. **45**, 471 (1998)
6. M. Xiao, Y.-Q. Li, S.-Z. Jin, J. Gea-Banacloche, Phys. Rev. Lett. **74**, 666 (1995)
7. N.P. Robins, B.J.J. Slagmolen, D.A. Shaddock, J.D. Close, M.B. Gray, Opt. Lett. **27**, 1905 (2002)
8. C. Wieman, T.W. Hänsch, Phys. Rev. Lett. **36**, 1170 (1976)
9. C.P. Pearman, C.S. Adams, S.G. Cox, P.F. Griffin, D.A. Smith, I.G. Hughes, J. Phys. B **35**, 5141 (2002)
10. K.L. Corwin, Z.T. Lu, C.F. Hand, R.J. Epstein, C.E. Wieman, Appl. Opt. **37**, 3295 (1998)
11. T. Petelski, M. Fattori, G. Lamporesi, J. Stuhler, G.M. Tino, Eur. Phys. J. D **22**, 279 (2003)
12. G. Wasik, W. Gawlik, J. Zachorowski, W. Zawadzki, Appl. Phys. B **75**, 613 (2002)
13. G.D. Rovera, G. Santarelli, A. Clairon, Rev. Sci. Instrum. **65**, 1502 (1994)
14. J.D. Jackson, *Classical Electrodynamics*, 3rd edn. (Wiley, 1999)
15. R. Loudon, *The Quantum Theory of Light* (Oxford University Press, 2000)
16. D.A. Smith, I.G. Hughes, Am. J. Phys. (to appear)